

Theoretical Study of Fair-Trade Sustainable Hatcheries - Sizing for Cameroon and Indonesia

Charles Awono ONANA¹, Jacques HONA², Laurent-Charles VALDÈS³

¹ Université des Montagnes, Bangangté, Cameroun

² Faculté des Sciences, Université de Yaoundé I, Yaoundé, Cameroun

³ Université Polytechnique Hauts-de-France, Valenciennes, France

Abstract

Fair-trade sustainable hatcheries are designed for developing and emerging countries, such as Cameroon and Indonesia respectively, so that they can use their often-generous sunshine at the service of harmonious development. These hatcheries are sustainable by their functioning exclusively from solar irradiation and nocturnal radiative emission. They are fair-trade because of their simplicity which allows them to be manufactured by many local professionals. They are developed so that the compensation in thermal losses is ensured by thermosiphon heat transfer loops thermo-regulated by bimetallic strip. These hatcheries are also designed for tropical or equatorial climatic hazards due to a fine modeling of physical phenomena which can also be implemented by using simple computer. An excellent economic return is expected.

Keywords: fair-trade sustainable hatchery; thermosiphon; bimetallic regulator; created entropy; liquid water

INTRODUCTION

Small or medium-scale hatching is a stimulus for the economy of developing and emerging countries, like Cameroon and Indonesia respectively, even if the operator has to use a generator or a photovoltaic installation [1], electricity being the mandatory intermediary of thermal regulation of commercial hatcheries or more experimental systems [2, 3]. The motivation for this study was to make a decisive improvement in this practice.

The hatcheries studied here for tropical-equatorial regions having been made independent from the electrical network by their heat or refrigeration storage loops circulating by thermosiphon and by their thermal regulation by bimetallic strip, they deserve the qualification of sustainable. Their description performed in the Experimental Design Section shows that their manufacturing accessibility also makes them the fair-trade products.

To further promote fairness, the software that allows their simulation has been adapted to the capabilities of simple personal computers, making their sizing accessible to smaller design offices. However, the reliability of the sizing having required forecasts of the calculation code which can compete in precision with those of popular softwares [4, 5, 6], particular care has been taken in posing the problem and in its resolution. Theoretical modeling is exposed in the Methods Section.

The fair-trade sustainable hatchery proposed in the Results and Discussion Section corresponds to a project developed with a view to implementation in Cameroon, but it turns out that the later is more convenient for Indonesia. This section also contains the results of the validation of the calculation code and returns to the decisive points.

EXPERIMENTAL DESIGN

General characteristics

The chick embryo is not overdue between the limits $\theta_{CO,min}=36^{\circ}C$ and $\theta_{CO,max}=38.8^{\circ}C$, the corresponding lethality limits being $34^{\circ}C$ and $39.4^{\circ}C$, respectively [7]. It is therefore between $\theta_{CO,min}$ and $\theta_{CO,max}$ that the temperature θ_{CO} in the incubation chamber, or incubator, must be maintained. In the countries where the room temperature θ'_{amb} still satisfies $\theta'_{amb} < \theta_{CO,min}$, there is sufficient to bring heat, but in the case where $\theta'_{amb} > \theta_{CO,max}$, an evacuation should be considered. In the first case, the hatcheries are only equipped with a heating device and called mono-loops. In the second case, with their additional cooling device, they are called bi-loops. The water of the "hot" loop of the fair-trade sustainable hatcheries flows through the incubator, a hot water tank and a solar collector. On the other hand, the water of the "cold" loop of the bi-loop hatcheries flows through the incubator, a cold water tank and a nocturnal radiator.

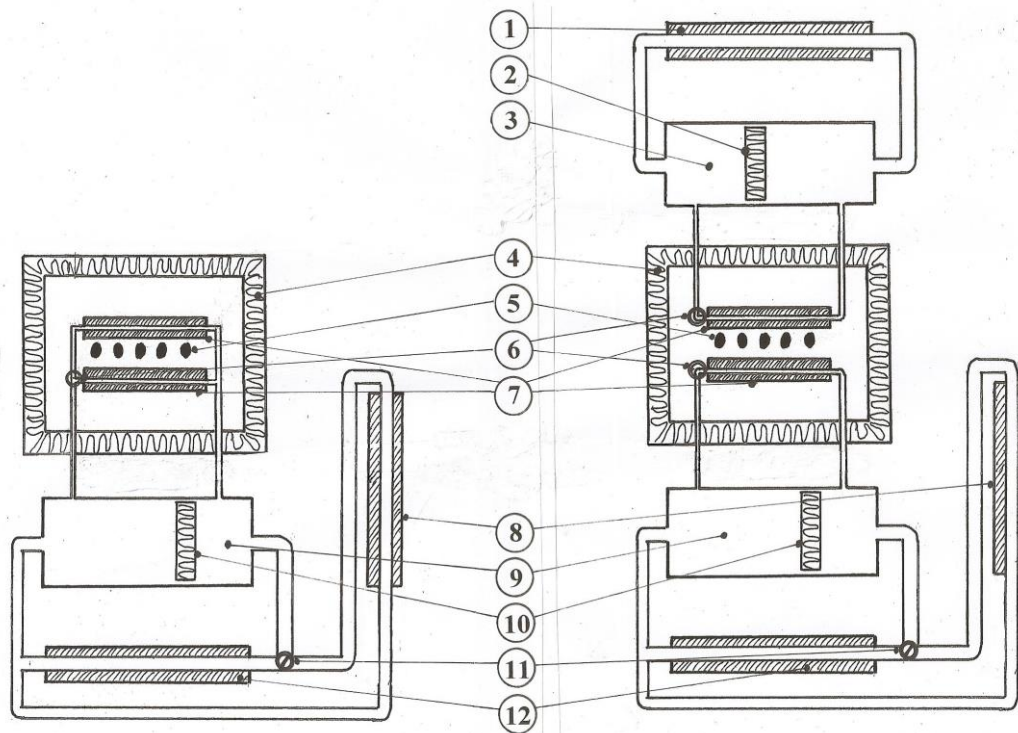


Figure 1. Schematic diagram of fair-trade sustainable mono-loop (left) and bi-loop (right) hatcheries.

1: nocturnal radiator, 2: cold separator, 3: cold water tank, 4: incubator, 5: eggs, 6: brooding regulator, 7: incubation exchanger, 8: heat discharge radiator, 9: hot water tank, 10: hot separator, 11: heat discharge regulator, 12: collector.

Figure 1 which shows the schematic diagram of fair-trade sustainable hatcheries reveals 1) the respective positions in altitude that the elements of the hatchery must have to trigger a spontaneous circulation of water when they are subjected to solar irradiation and the nocturnal radiative emission, 2) the heat discharge radiator 8, grafted onto the hot regeneration sub-loop to prevent it from overheating, as well as 3) regulators by thermo-regulated lamination at the outlet of the

incubator 6 and collector 11 driven by bimetallic strips wound in a helix, or bimetallic-helices.

Constructive provisions

Construction materials. The hatchery is presented as an assembly, around a sheet steel box, of PVC pipes, elbows, tees (pipes) and tubes (tanks) as well as corrugated sheet heat exchangers, these elements being fixed on a wooden structure as shown in Fig. 2.

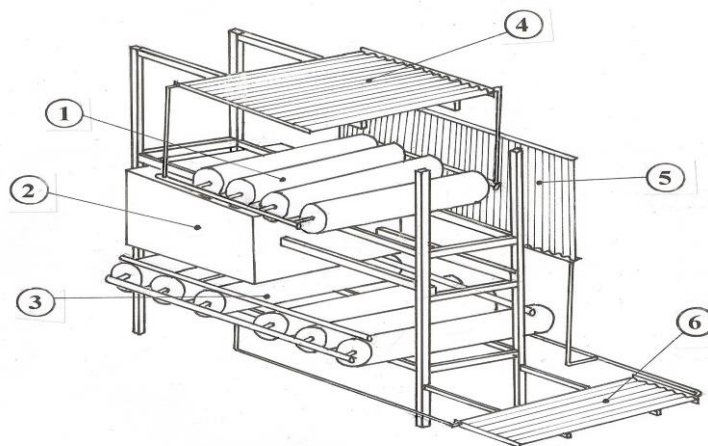


Figure 2. Overview of fair-trade sustainable hatcheries.

1: cold water tank, 2: rear opening incubator, 3: hot water tank, 4: nocturnal radiator, 5: heat discharge radiator, 6: collector in front.
Mono-loop case without 1 nor 4. Discharge radiators 5 on the right side not shown.

Overall configuration. From top to bottom, one finds the radiator 4, the cold-water tank 1, the incubator 2, the hot water tank 3 and the collector 6, radiator and cold-water tank less in the mono-loop hatcheries. These elements are superimposed, except for the collector which is shifted forward. The two heat discharge radiators 5 are on the sidewalls.

The wooden structure that supports these elements is made up of four vertical uprights secured by five cross members (three in front and two behind) and four longitudinal members, two of which (mono-loops) or four (bi-loops) support the water tanks. At the bottom, two cantilevered longitudinal members support the collector.

Halfway up, two longitudinal members resting on the central cross member at the front and on two short uprights at the rear, support the incubator. At the top, two longitudinal members support the radiator of the bi-loop hatcheries.

Heat exchangers. Each exchanger consists of two corrugated sheets superimposed and offset laterally to clamp the water inlet and outlet pipes (Fig. 3). Their mutual fixing was done by riveting on their contact generatrice and the open faces are closed by a strip cut in the corrugated sheet, pre-drilled for the passage of the PVC tubes and welded at the end. The exchanger thus appears as a set of parallel channels.

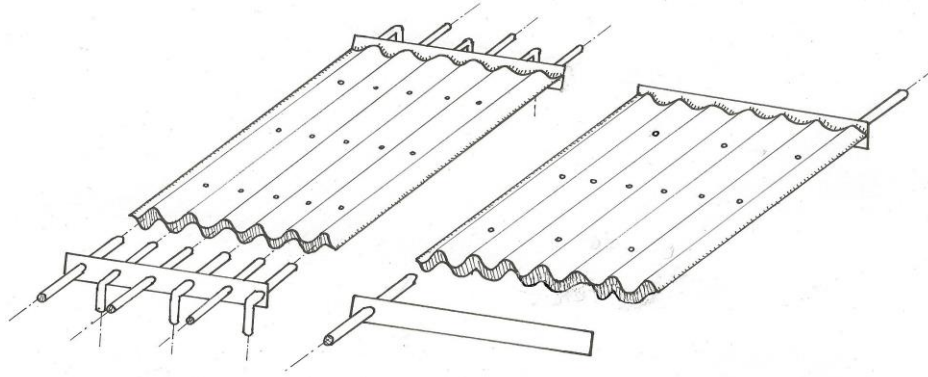


Figure 3. Corrugated sheet heat exchangers.

Incubator exchanger with parallel circulation in alternating directions (left), collector and coil radiators (right).

In the in even number channels of the incubator, the water inlet flow is divided and organized to cross them in parallel and in alternating directions, supply and discharge being ensured by a tube clamped at each end, overlooking a wet nurse (Fig. 4). In the in odd

number channels of the collector and radiators, the water flow follows a path configured as a serpentine, the exchanger ends having been moved apart before the sealing strips are welded.

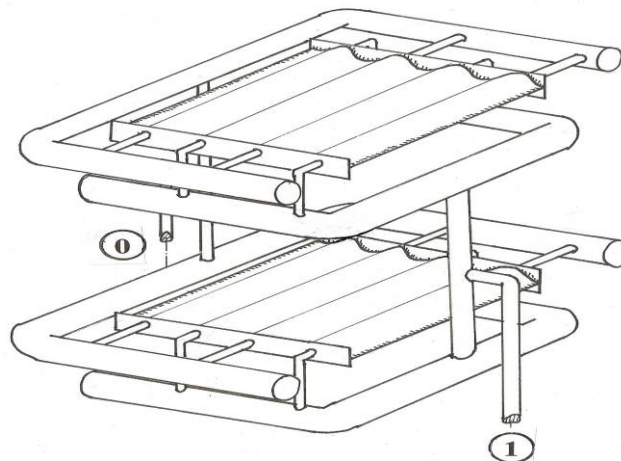


Figure 4. Incubator heat exchanger - Mono-loop version.

Water admission (or return) by 1 then by the two lower wet nurses and return (or admission) by 0 then by the two upper wet nurses, simultaneously in the two layers.

Incubator. In its center is a bottomless drawer, closed on both sides by a removable mesh. The eggs are packed there in parallel rows by separating boards. When the drawer is out, the eggs can be turned all together by rotating the drawer around a horizontal axis caught between its slides. These are extended to collect the overhang of the drawer. When the drawer is in, they exit through the back of the incubator. The egg drawer is then located between the two heat exchangers according to Fig. 4. In mono-loop configuration, all the channels are traversed by water from the hot loop and only one out of two channels in bi-loop configuration, the other being by the water of the cold loop. An open water tank is installed at the bottom of the incubator. The latter is delimited by a double insulated metal casing internally. The sides facing the heat insulator are reflective, the inner face is painted black, and the outer face is light and in the shade.

Tanks. They are made of large diameter PVC tubes, closed at their ends and insulated. A thick disc with the inside diameter of the tubes, cut from an insulating material of the expanded polystyrene type and ballasted by a metal weight to communicate the water flotation to it, or separator, separates, inside each tank tube, the regenerated water from the return of the

incubator (Fig. 1). The regeneration sub-loops are connected to their reserve at the level of the axis of the tube bottoms and the incubation sub-loops, at the ends of these tubes, on the upper generatrix (hot loop) or lower (cold loop) (Fig. 1).

Collector and radiators. The collector and the nocturnal radiator of the bi-loop hatcheries are placed horizontally. The two heat discharge radiators are placed vertically along the sidewalls, raised above the collector. The collector and the three radiators are completely painted black. The absorbent face of the collector is exposed under glass.

Bimetallic regulators. The brooding regulator uses two parallel bimetallic helices, placed at the top of the incubator, whose rotations control, at the end of a lever arm, the reverse vertical translations of two cylindrical half-shutters (Fig. 5). In mono-loop hatcheries, the free end is attached to the support tube. In bi-loop hatcheries, both ends control a shutter system are similar to that previously described; two stops and a return spring make it possible to switch from the active mode of the hot loop at low temperatures with closing of the cold loop, to that of the cold loop at high temperatures with closing of the hot loop.

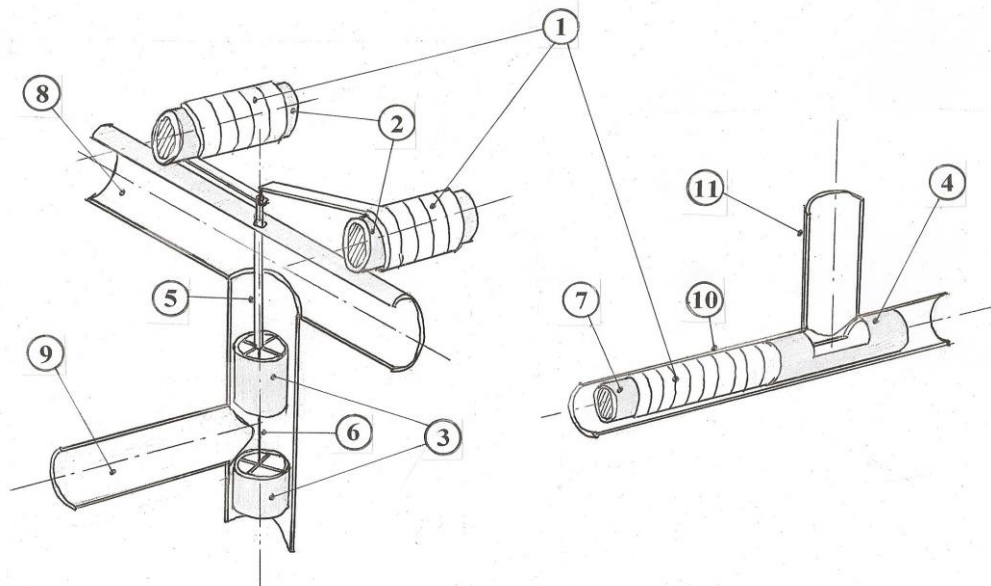


Figure 5. Incubation (left) and heat discharge (right) bimetallic-helix regulators.

1: bimetallic trip, 2: bimetallic support tube, 3: cylindrical shutter, 4: semi-cylindrical shutter, 5: suspension tube, 6: suspension wire, 7: rotating stop section, 8: upper incubator outlet wet nurse, 9: incubator outlet pipe, 10: main pipe, 11: bypass pipe.

The heat discharge regulator is a bimetallic-helix bathed in the flow of the output of the collector. One end is fixed (Fig. 5) and the other controls the rotation of the semi-cylindrical shutter for deflecting the main flow.

Thermosiphon initiators. They present themselves in the form of a bundle of rods that are good heat conductors (aluminum) and are positioned at the four connections of the tank tubes with the regeneration and incubation sub-loops, straddling the tank tube and the concerned pipeline. The separator has a thickness slightly greater than the diameter of the openings which open into the incubation sub-loop; in its extreme positions, it hides them completely.

Operation. The fair-trade sustainable hatcheries in the bi-loop version must, on their own, be operated when the room temperature can exceed $\theta_{CO,max}=38.8^{\circ}C$. All of them work outdoors, facing north-south, with the collector pointing towards the other hemisphere of the earth.

Users of fair-trade sustainable hatcheries would be bound by the precautions and care in use

with hatcheries: eggs previously fertilized and turning over several times a day. Adding humidification water to the tank is done by compensating for the slight water leak at the level of the brooding regulator.

METHODS

External temperatures. The temperature T_j'' is expressed from the Stefan-Boltzmann formula by

$$(1) \quad T_j'' = (\Phi_{CC} / (\rho\sigma))^{1/4}.$$

It is obtained from solar fluxes Φ_{CC} (cloudy sky) and Φ_{CD} (clear sky), as well as from ρ (soil albedo) and τ_{deg} (fraction of clear sky) on the basis of the methods of Schuepp [8]:

$$\Phi_{CC} = \Phi_{CD} \cdot \left[\rho + (1 - \rho) \cdot \sqrt{(\tau_{deg} + \tau_{deg}^2) / 2} \right] \quad \text{and}$$

Perrin de Brichambaut and Dogniaux [8]:

$$\Phi_{CD} = \Phi_0 \cdot A \cdot \left[\frac{Tr}{31.6 \cdot \sqrt{\cos(L - \delta)}} + \exp \left[\frac{Tr}{7.5 \cdot \sqrt{\cos^{1.5}(L - \delta)}} \right] \right]$$

by setting

$$\begin{cases} A = \sqrt{\cos^2(L) \cdot \cos^2(\delta) - \sin^2(L) \cdot \sin^2(\delta)} / \arccos\{\tan(L) \cdot \tan(\delta)\} + \sin(L) \cdot \sin(\delta) \\ Tr = 2.5 + 14.8 \cdot \beta + 0.4 \cdot (1 + 2 \cdot \beta) \cdot \ln[W] \\ W = 170 \cdot A \cdot \exp[56.535 - 7218/T_j' - 6.278 \cdot \ln(T_j'')] \end{cases}$$

where L is the latitude and $\beta=0.05, 0.1$ or 0.2 depending on the environment, rural, urban or industrial of the forecast.

The temperature T_N'' , obtained by

$$(2) \quad T_N'' = \tau_{deg} \cdot (0.0552 \cdot T_N'^{3/2}) + (1 - \tau_{deg}) \cdot (T_N' - 6 \text{ K})$$

is based on Swinbank

$$T_N'' = 0.0552 \cdot T_N'^{3/2}$$

and Whillier

$$T_N'' = T_N' - 6 \text{ K}$$

correlations [9].

Table 1. Nomenclature.

Symbol	Description
θ_{CO} / $\theta_{CO,min}$ / $\theta_{CO,max}$	temperature ($^{\circ}C$) in the incubator / minimum / maximum border
θ'_{amb} / θ'_j / θ'_N	convective temperature ($^{\circ}C$) of the room / diurnal / nocturnal atmosphere
T'_{amb} / T'_j / T'_N	convective temperature (K) of the room / diurnal / nocturnal atmosphere
T''_{amb} / T''_j / T''_N	radiative temperature (K) of the room / diurnal / nocturnal atmosphere
σ	Boltzmann constant: $\sigma = 5.67 \cdot 10^{-8} \text{ W} \cdot \text{m}^{-2} \cdot \text{K}^{-4}$
Φ_0	solar flux constant outside the atmosphere: $\Phi_0 = 1353 \text{ W} \cdot \text{m}^{-2}$
δ	angle between the equatorial plane and the ecliptic plane: $\delta = 23.26^{\circ}$
e_{bil} / l_{bil}	thickness / width of the bimetallic strips
l_{bil}^{inc} / l_{bil}^{dech}	bimetallic strip length of the incubation / heat discharge regulator
T_j / T_N	temperature (K) of the absorber (collector) / emitters (radiator)
c_{eau}	stall constant: $c_{eau} = 3614 \text{ J} \cdot \text{kg}^{-1} \cdot \text{K}^{-1}$
Δt_{cyc} / Δt_{RG}	duration of the daily cycle (86 400 s) / of the regeneration
A_j	projected area of the collector
α / α_{ext} / α_{CO}	global heat exchange coefficient / of the external source / incubator
A / A_{ext} / A_{CO}	area of the heat exchange surface / of the external source / incubator
H_C	height of regeneration driving
$\Delta\theta = \theta_j - \theta_{CO}$	temperature difference between heat sources
c	water velocity in regeneration pipes
\dot{Q}_e	heat power transferred by the thermosiphons in the considered loop
M	mass of water in circulation in a daily cycle or in the considered hot or cold loop tank
V_{vent}	wind velocity
H_{AV} / H_{AR}	uprights height at the front / rear
L / l	length / width of the wooden structure
L_{cap} / L_{inc}	length of collector members / incubator support uprights
L_{CO} / l_{CO} / H_{CO}	internal length / width / height of the incubator
\tilde{L}_{CO} / \tilde{l}_{CO} / \tilde{H}_{CO}	external length / width / height of the incubator
L_N / N_N	length / number of corrugations of the nocturnal radiator
L_j / N_j	length / number of corrugations of the collector
L_D / N_D	length / number of corrugations of heat discharge radiators
$L_{Re,S,C}$ / $N_{Re,S,C}$	length / number of hot reserve tubes
$L_{Re,S,F}$ / $N_{Re,S,F}$	length / number of cold reserve tubes
d_{CO} / D_{CO}	external diameter of the pipe / incubator wet nurse
d_{RG} / D_{RG}	external diameter of the pipe / regeneration wet nurse
D_{Res}	external diameter of the tubes of the water tanks
$e_{isol,CO}$ / $e_{isol,Res}$ / $e_{isol,Tub}$	thickness of the heat insulation on the incubator / reserves / PVC pipes

Regulators

Principle of regulation. The free ends of a bimetallic helix are positioned at an angle proportional to the temperature. By translating a cylindrical shutter at the end of a lever arm (brooding regulators) or by driving a semi-

cylindrical shutter in rotation (heat discharge regulators) (Fig. 5), they gradually open or close the section of fluid passage between the listed boundaries in Table 2 where $\bar{\theta}_{CO} = (\theta_{CO,max} + \theta_{CO,min})/2$.

Table 2. Thermal conditions related to the regulators.

bimetallic strip on	Full opening	Complete closure
discharge circuit	$\theta_1 \geq \theta_{1,max}$	$\theta_1 \leq \theta_{1,min}$
hot loop / mono-loop	$\theta_{CO} \leq \theta_{CO,min}$	$\theta_{CO} \geq \theta_{CO,max}$
hot loop / bi-loop	$\theta_{CO} \leq \theta_{CO,min}$	$\theta_{CO} \geq \bar{\theta}_{CO}$
cold loop	$\theta_{CO} \geq \theta_{CO,max}$	$\theta_{CO} \leq \bar{\theta}_{CO}$

θ_1 for the temperature of the water at the collector outlet (Fig. 6); $\theta_{1,min}$ and $\theta_{1,max}$ for its lower and upper borders.

Sizing of the regulators

It is performed on the basis of the relationship $\Delta\alpha = 360^\circ/\pi \cdot (R \cdot L_{bil} \cdot \Delta\theta)/e_{bil}$ pertaining to the bimetallic-helices' theory [10], where L_{bil} is the length of the bimetallic strip (developed length), R its specific rotation and $\Delta\alpha$ its rotation under the temperature difference $\Delta\theta$.

The length L_{bil}^{dech} is obtained by applying this relationship with a 90° rotation as the temperature changes from $\theta_{1,min}$ to $\theta_{1,max}$. We obtain

$$(4) \quad L_{bil}^{dech} = \pi \cdot e_{bil} / (4 \cdot R \cdot (\theta_{1,max} - \theta_{1,min})).$$

For the length L_{bil}^{inc} , a translation condition of a half-diameter $d_{i,RG}$ of the pipe to be closed at the end of the lever arm r , leads, for a diameter helix d , to

$$(5) \quad L_{bil}^{inc} = \sqrt{\pi/2 \cdot e_{bil} \cdot d / (R \cdot \Delta\theta)} \cdot d_{i,RG} / l_{bil},$$

where $\Delta\theta = \theta_{CO,max} - \theta_{CO,min}$, $\Delta\theta = \bar{\theta}_{CO} - \theta_{CO,min}$ or $\Delta\theta = \theta_{CO,max} - \bar{\theta}_{CO}$, according to Table 2.

An elementary geometry calculation leads to the expression:

$$(6) \quad A_{dech} = \pi \cdot \frac{d_{i,RG}^2}{4} \cdot \left[\frac{\theta_1 - \theta_{1,min}}{\theta_{1,max} - \theta_{1,min}} - \frac{1}{2\pi} \sin\left(2\pi \cdot \frac{\theta_1 - \theta_{1,min}}{\theta_{1,max} - \theta_{1,min}}\right) \right]$$

of the area A_{dech} of the cross section offered to the discharge flow as a function of θ_1 and to that

$$(7) \quad A_{CO} = \frac{d_{i,RG}^2}{2} \cdot \left[\arcsin\left(\frac{\theta_{CO,max} - \theta_{CO}}{\theta_{CO,max} - \theta_{CO,min}}\right) + \frac{\theta_{CO,max} - \theta_{CO}}{\theta_{CO,max} - \theta_{CO,min}} \cdot \sqrt{1 - \left(\frac{\theta_{CO,max} - \theta_{CO}}{\theta_{CO,max} - \theta_{CO,min}}\right)^2} \right]$$

of the area A_{CO} of the straight section offered to the brooding flow as a function of θ_{CO} .

Heat transfers

Incubator. The heat sources of its thermal model are the heat transfer fluid circulating 1) at temperature T_e in the admission wet nurse, 2) at temperature \bar{T} in the exchangers and 3) at temperature T_s in the return wet nurse (Fig. 4), 4) the interior of the incubator at temperature T_{CO} , the room atmospheres 5) at T'_{amb} and 6) at T''_{amb} ; the temperature $T_{p,inc}$ of the outer enclosure wall appears as an intermediate unknown.

The overall conductance between the heat transfer fluid and the parts at temperature T_{CO} is the sum of those between the fluids at temperature T_e , at temperature \bar{T} and at temperature T_s , and the set at temperature T_{CO} ; it is affected by a factor of $1/2$ when the incubator is of the bi-loop type. All three involve forced internal convection between the heat transfer fluid and the internal wall (exchangers and pipes). The external wall of the exchanger transmits heat by radiation and natural convection. The conductance through the pipes involves conduction in the PVC wall and natural convection outside. The conductance between the parts at temperature T_{CO} and the atmosphere takes into account the conduction in the insulation, the radiation and the convection, forced or natural depending on the wind velocity, on the wall of the outer enclosure.

Collector. The heat sources of its thermal model are 1) the heat transfer fluid at temperature \bar{T} and the room atmospheres 2) at temperature T'_j and

3) at temperature T_J'' towards the sun (T_J' towards the ground); the temperatures T_J , $T_{p,vitre}$ of the outer glazed face and T_{ssabs0} of the shadowy face appear to be intermediate unknowns.

The conductance between the heat transfer fluid and the absorber comes from forced internal convection. That between the absorber and the atmospheric sources takes into account the incident radiation from the source at temperature T_J'' , the conduction in the air space enclosed by the glass, the mutual radiation between the absorber and the glass, the conduction in the glass, as well as the radiation and convection, forced or natural depending on the wind velocity, on the glass. The conductance on the shaded face includes forced convection with the heat transfer fluid, mutual radiation, and convection, forced or natural depending on the wind velocity.

Nocturnal radiator. The heat sources of its thermal model are 1) the heat transfer fluid at temperature \bar{T} , the room atmosphere 2) at temperature T_N' and 3) at temperature T_N'' towards the sky (T_N' towards the ground); the temperature T_N of the assumed isothermal walls of the radiator appears as an intermediate unknown.

The conductance between the heat transfer fluid and the internal wall of the exchanger comes from internal forced convection. That between the external walls and the atmospheric sources includes the radiation and the convection, forced or natural according to the wind velocity, of the walls.

Discharge radiators. The thermal model uses that of the nocturnal radiator, replacing T_N' with T_{amb}' and T_N'' with T_{amb}'' . The conductance between outer walls and atmospheric sources includes radiation on both faces, external forced convection and natural convection on the outward facing sides and the incubator, respectively.

Heat transfers. The conductances relative to the thermal models are available at the authors. They

are obtained on the basis of formulas and correlations well known by thermal engineers [11].

Thermosiphon

Thermodynamic model of liquid water. Based on the results of Table 3 and the equation of state of basic form:

$$(8) \quad v = v_0 \cdot (1 + \alpha_0 \cdot T + \alpha_1 \cdot T^2) \cdot (1 + \chi_T \cdot p)$$

with v , T and p for the mass volume, temperature and pressure of water, the least mean squares technique having provided

$$v_0 = 1.30859 \cdot 10^{-3} \text{ m}^3 \cdot \text{kg}^{-1},$$

$$\alpha_0 = 1.74780 \cdot 10^{-3} \text{ K}^{-1}, \quad \alpha_1 = 3.23605 \cdot 10^{-6} \text{ K}^{-2}$$

$$\text{and } \chi_T = 2.18979 \cdot 10^{-9} \text{ bar}^{-1}.$$

Associated with a specific heat capacity at constant volume c_v of the form

$$c_v = c_{eau} - \frac{T}{\chi_T} \cdot \frac{v^2}{2 \cdot v_0} \cdot \frac{d}{dT} \left[\frac{\alpha_0 + 2 \cdot \alpha_1 \cdot T}{(1 + \alpha_0 \cdot T + \alpha_1 \cdot T^2)^2} \right] \text{ to make}$$

the differential forms $c_v \cdot dT + (l_v - p) \cdot dv$ and $c_v/T \cdot dT + l_v/T \cdot dv$ exact, the equation of state (8) allows, by integration, to obtain the expressions of the internal mass energy

$$u(T, v) = c_{eau} \cdot T + \frac{1}{\chi_T} \cdot v$$

$$(9) \quad \dots - \frac{1}{\chi_T} \cdot \frac{1 + 2 \cdot \alpha_0 \cdot T + 3 \cdot \alpha_1 \cdot T^2}{(1 + \alpha_0 \cdot T + \alpha_1 \cdot T^2)^2} \cdot \frac{v^2}{2 \cdot v_0} \\ \dots + u_0$$

and the mass entropy

$$s(T, v) = c_{eau} \cdot \ln(T)$$

$$(10) \quad \dots - \frac{1}{\chi_T} \cdot \frac{\alpha_0 + 2 \cdot \alpha_1 \cdot T}{(1 + \alpha_0 \cdot T + 2 \cdot \alpha_1 \cdot T^2)^2} \cdot \frac{v^2}{2 \cdot v_0} \\ \dots + s_0$$

from where that of the mass enthalpy

$$h(T, v) = c_{eau} \cdot T$$

$$(11) \quad \dots + \frac{1}{\chi_T} \cdot \frac{1 - \alpha_1 \cdot T^2}{(1 + \alpha_0 \cdot T + \alpha_1 \cdot T^2)^2} \cdot \frac{v^2}{2 \cdot v_0} \\ \dots + h_0$$

Table 3. Mass volume of water in terms of $10^{-3} \text{ m}^3 \cdot \text{kg}^{-1}$ at several temperatures and two pressures [12].

pressure	temperatures				
	0°C	20°C	40°C	60°C	80°C
1 bar	1.0000	1.0016	1.0076	1.0168	1.0287
500 bar	0.9767	0.9804	0.9867	0.9967	1.0071

Modeling of loops. The loops are modeled on a stationary daily cycle, involving masses of water having passed through the incubator and the regenerator equal, and during which the operating

conditions are assumed to be constant. The presence of the movable separator disc, without friction and insulating, makes it possible to look at each compound loop (Fig. 6) as the succession of

parts 1-2, 2-3, 3-4, 4-4', 4'-1' and 1'-1 defined by constant states, despite the movement of the separator.

Depending on the calculation cycle, the water circulates separately in the incubation 1-2-3-4 and regeneration 4-4'-1'-1 sub-loops, but the circulations of incubation (slow and continuous movement of the separator from 4 to 1) and of regeneration (rapid movement from 1 to 4 as long as the collector is sufficiently hot or the radiator, sufficiently cold) are globalized by the integration of the equations on the daily cycle. Simple loops are modeled by the parts 2-3, 3-4', 4'-1' and 1'-2.

The variations in kinetic energy through the parts, zero or insignificant, are neglected.

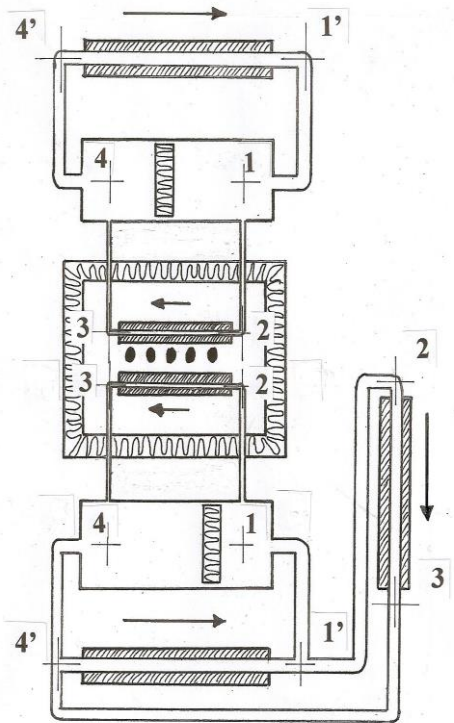


Figure 6. Thermosiphon loops.

Note: 1: horizontal plane of symmetry of the tank on the regenerated water side, 2: inlet section of the incubation exchanger or heat discharge radiator, 3: outlet section of the incubation exchanger or heat discharge radiator, 4: horizontal plane of symmetry of the tank on the incubation return water side, 4': inlet section of the regeneration exchanger and 1': outlet section of the regeneration exchanger.

Equations related to the parts. The equality $\dot{M}_s = -\dot{M}_e$ between outgoing and incoming flows (stationary mass balance) is implicit.

The assumption of the linear variation $v(p) = v_e + (v_s - v_e)(p - p_e)/(p_s - p_e)$ between input e and output s leading to $\int_{p_e}^{p_s} v \cdot dp = (v_s + v_e)(p_s - p_e)/2$ is accepted to

make the stationary mechanical energy balance equation applicable (Bernoulli)

$\int_{p_e}^{p_s} v \cdot dp + (c_s^2 - c_e^2)/2 + g \cdot (z_s - z_e)$. It leads to the

relation of: $\dots = w_{i,e \rightarrow s} + w_{f,e \rightarrow s}^L + w_f^0$

$$(12) \quad (v_s + v_e) \cdot (p_s - p_e)/2 + g \cdot (z_s - z_e) \dots = w_{f,e \rightarrow s}^L + w_f^0$$

suitable to the rigid parts studied ($w_{f,e \rightarrow s}^L$ and w_f^0 below).

The equations of total energy balance $dE/dt = \dot{W} + \dot{Q}_e + \sum_{trfj} (h_i + c_i^2/2 + g \cdot z_i) \dot{M}_i$ [13]

and of entropy balance $dS/dt = \sum_{scej} \dot{Q}_e/T_j + \sum_{i=1}^I s_i \cdot \dot{M}_i + \dot{S}^r$ [14] become, in the

present case of stationary flows in rigid parts, in thermal contact with at most one source exchanging $q_{e,e \rightarrow s}$ between e and s

$$(13) \quad 0 = q_{e,e \rightarrow s} + h_e - h_s + g \cdot z_e - g \cdot z_s \text{ and}$$

$$(14) \quad 0 = q_{e,e \rightarrow s}/T_j + s_e - s_s + s_{W,e \rightarrow s}^r + s_{Q,e \rightarrow s}^r$$

respectively ($s_{W,e \rightarrow s}^r$ and $s_{Q,e \rightarrow s}^r$ below).

Pressure drops. The general expression $w_{f,e \rightarrow s}^L = -\xi \cdot c^2/2 \cdot L/d_h$ of the mass work of viscous friction by linear pressure drop in a pipe of hydraulic length L and diameter d_h becomes, in laminar regime written as $\xi = 64/Re$ [15]:

$$(15) \quad w_{f,e \rightarrow s}^L = -128/\pi \cdot \bar{\eta} \cdot \bar{v}^2 \cdot L/d_h^4 \cdot M/\Delta t ;$$

that of the mass work of viscous friction $w_f^0 = -\xi_0 \cdot c^2/2$ by singular pressure drop in the section of index 0 becomes, with $\xi = 2 \cdot (1 - A_0/A_1)$ for the diaphragm with straight edges [15],

$$(16) \quad w_f^0 = -0.25 \cdot (1 - 4 \cdot A/(\pi \cdot d_i^2)) \cdot (v_i \cdot M/(A \cdot \Delta t))^2$$

in the case of an open area A in the pipe diameter d_i . Δt is the duration of circulation, to be specified according to brooding (Δt_{cyC}) or regeneration (Δt_{RG}).

Created entropies. The entropy expression $s_{W,e \rightarrow s}^r$, created by lamination, is established from the formula $\delta s_W^r = -\delta w_f/T$. In the case of a singular pressure drop in a section of index 0, it is immediate that

$$(17) \quad s_{W,e \rightarrow s}^0 = -w_f^0/T_0 ,$$

and in that of a linear pressure drop, integration along the pipe gives

$$(18) \quad s_{W,e \rightarrow s}^L = -w_{f,e \rightarrow s}^L \cdot \ln(T_s/T_e)/(T_s - T_e) .$$

The entropy expression $s_{Q,e \rightarrow s}^f$, created by heat transfer between the fluid at temperature T and a heat source at temperature T_{sce} , is established from

$s_{Q,e \rightarrow s}^f = -\alpha \cdot \int_0^A (1/T - 1/T_{sce}) \cdot (T - T_{sce}) \cdot dA$ thanks to Newton's law $\delta q_e = -\alpha \cdot dA \cdot (T - T_{sce})$ assumed here. The law $T(A)$ is obtained by writing the local total energy balance in the exchanger $0 = -\dot{M} \cdot (dh/dT) \cdot dT - \alpha \cdot dA \cdot (T - T_{sce})$ within the framework of current thermodynamic model of water above. The calculation leads, with an approximation to order 1, to:

$$(19) \quad s_{Q,e \rightarrow s}^f = \frac{c_{eau}}{P} \cdot \left[(1 + Q \cdot T_{sce}) \cdot \ln \left(\frac{T_{sce} + (T_e - T_{sce}) \cdot \exp\left(-\frac{\Gamma \cdot \Delta t}{M \cdot c_{eau}} \cdot P\right)}{T_e} \right) + \dots \right. \\ \left. \dots + \left(1 + \frac{1}{Q \cdot T_{sce}}\right) \cdot \ln \left(\frac{T_{sce} + (T_e - T_{sce}) \cdot \exp\left(-\frac{\Gamma \cdot \Delta t}{M \cdot c_{eau}} \cdot P\right)}{(1 - Q \cdot (T_e - T_{sce})) \cdot T_s} \right) \right]$$

by setting $P = \frac{1 + \frac{\alpha_1 \cdot v_0 \cdot M}{\chi_T \cdot \alpha \cdot A \cdot \Delta t} \cdot (1 + \chi_T \cdot p_e)^2 \cdot T_e}{1 - \frac{\alpha_1 \cdot v_0 \cdot M}{\chi_T \cdot \alpha \cdot A \cdot \Delta t} \cdot (1 + \chi_T \cdot p_e)^2 \cdot T_{sce}}$,

$$Q = \frac{\frac{\alpha_1 \cdot v_0}{\chi_T \cdot c_{eau}} \cdot (1 + \chi_T \cdot p_e)^2}{1 - \frac{\alpha_1 \cdot v_0 \cdot M}{\chi_T \cdot \alpha \cdot A \cdot \Delta t} \cdot (1 + \chi_T \cdot p_e)^2 \cdot T_{sce}}$$
 and introducing

the inductance $\Gamma = \alpha \cdot A$.

Mechanical equilibrium of the separator disc. The mechanical energy balance equation shows that the equilibrium of the disc takes place for $p_1 = p_4$ (pressures on the axis of the tank).

Resolution of the thermosiphon of a compound loop

Method. The loop balance equations for mechanical energy and entropy are included in the system to be solved with the balance equations for the parts that are not overabundant. With the conditions $q_{e,2 \rightarrow 3} = -q_{e,4' \rightarrow 1'}$ and $p_1 = p_4 = p_{atm}$ reflecting the total energy balance of the loop and the mechanical equilibrium of the separator disc, the thermosiphon of the loop is described by the solution in M , $q_{e,4' \rightarrow 1'}$, T_1 , T_2 , T_3 , T_4 , $T_{4'}$, $T_{1'}$, p_2 , p_3 , $p_{4'}$, $p_{1'}$ of the system where the expressions of the quantities $w_{f,e \rightarrow s}^L$ and w_f^0 are given by Eqs. (15) and (16), respectively. On the other hand, the expressions of the quantities $s_{W,e \rightarrow s}^L$, s_W^0 and $s_{Q,e \rightarrow s}^f$ are given by Eqs. (17),

(18) and (19), respectively. Moreover, the expressions of the quantities $v(T, p)$, $s(T, p)$ and $h(T, p)$ are given by the Eqs. (8), (10) and (11), respectively.

$$(20) \quad \left\{ \begin{array}{l} \text{Emec_loop} = \sum_{e \rightarrow s} 2 \cdot g \cdot (z_s - z_e) / (v_s + v_e) + \dots \\ \dots - \sum_{e \rightarrow s} 2 \cdot w_{f,e \rightarrow s}^L / (v_s + v_e) - 2 \cdot w_f^0 / (v_1 + v_f) - 2 \cdot w_f^0 / (v_3 + v_4) = 0 \\ \text{Emec2_3} = (v_2 + v_3) \cdot (p_3 - p_2) / 2 - w_{f,2 \rightarrow 3}^L = 0 \\ \text{Emec3_4} = (v_3 + v_4) \cdot (p_{atm} - p_3) / 2 + g \cdot (z_4 - z_3) - w_{f,3 \rightarrow 4}^L = 0 \\ \text{Emec4_1'} = (v_{4'} + v_{1'}) \cdot (p_{1'} - p_{4'}) / 2 - w_{f,4' \rightarrow 1'}^L = 0 \\ \text{Emec1_1} = (v_{1'} + v_1) \cdot (p_{atm} - p_{1'}) / 2 + g \cdot (z_1 - z_{1'}) - w_{f,1 \rightarrow 1'}^L = 0 \\ \text{Entr_loop} = \sum_{e \rightarrow s} s_{W,e \rightarrow s}^L + \sum_{e \rightarrow s} s_{Q,e \rightarrow s}^f - \dots \\ \dots - q_{e,4' \rightarrow 1'} / T_{CO} + q_{e,4' \rightarrow 1'} / T_{sce} + s_{1'}^f + s_{3'}^f = 0 \\ \text{Entr2_3} = -q_{e,4' \rightarrow 1'} / T_{CO} + s_{W,2 \rightarrow 3}^f + s_{Q,2 \rightarrow 3}^f + (s_2 - s_3) = 0 \\ \text{Entr3_4} = s_{W,3 \rightarrow 4}^f + s_{3'}^f + (s_3 - s_4) = 0 \\ \text{Entr4_1'} = q_{e,4' \rightarrow 1'} / T_{sce} + s_{W,4' \rightarrow 1'}^f + s_{Q,4' \rightarrow 1'}^f + (s_{4'} - s_{1'}) = 0 \\ \text{Entr1_1} = s_{W,1 \rightarrow 1'}^f + s_{1'}^f + (s_1 - s_{1'}) = 0 \\ \text{Etot2_3} = -q_{e,4' \rightarrow 1'} + (h_2 - h_3) = 0 \\ \text{Etot4_1'} = q_{e,4' \rightarrow 1'} + (h_{4'} - h_{1'}) = 0 \end{array} \right.$$

The set of Eq. (20) above is solved by using the Newton-Raphson method [16].

Shaping of the starting point. The starting values of the unknowns of Eq. (20) are obtained by an approximate resolution. Water is assimilated there to an ideal condensed body. The compound loop is reduced to the simple loop as shown in Fig. 6, supplemented by the assumptions of isothermal adiabatic changes at temperatures T_2 and $T_{4'}$ (entering and leaving the incubator), with pressure $p_2 = p_{atm}$ and of heats exchanged equal and opposite; we obtain (21):

$$\left\{ \begin{array}{l} T_2 = \frac{T_{sce} \cdot \left(1 - \exp\left(-\frac{\Gamma_{sce} \cdot \Delta t_{sce}}{M \cdot c_{eau}}\right)\right) + T_{CO} \cdot \exp\left(-\frac{\Gamma_{sce} \cdot \Delta t_{sce}}{M \cdot c_{eau}}\right) \cdot \left(1 - \exp\left(-\frac{\Gamma_{CO} \cdot \Delta t}{M \cdot c_{eau}}\right)\right)}{1 - \exp\left(-\frac{\Gamma_{CO} \cdot \Delta t + \Gamma_{sce} \cdot \Delta t_{sce}}{M \cdot c_{eau}}\right)} \\ T_{4'} = \frac{T_{sce} \cdot \exp\left(-\frac{\Gamma_{CO} \cdot \Delta t}{M \cdot c_{eau}}\right) \cdot \left(1 - \exp\left(-\frac{\Gamma_{sce} \cdot \Delta t_{sce}}{M \cdot c_{eau}}\right)\right) + T_{CO} \cdot \left(1 - \exp\left(-\frac{\Gamma_{CO} \cdot \Delta t}{M \cdot c_{eau}}\right)\right)}{1 - \exp\left(-\frac{\Gamma_{CO} \cdot \Delta t + \Gamma_{sce} \cdot \Delta t_{sce}}{M \cdot c_{eau}}\right)} \end{array} \right.$$

for $\Gamma_{sce} = \alpha_{sce} \cdot A_{sce}$ (heat source) and $\Gamma_{CO} = \alpha_{CO} \cdot A_{CO}$ (incubator or heat discharge radiator).

The resolution is done at temperature T_2 , by dichotomy. Each iteration proceeds in two stages: 1) determination of the mass M from Eq. (21), 2) approximation of the heat $q_{e,4' \rightarrow 1'}$ by $q_{e,4' \rightarrow 1'} = h(T_2, p_2) - h(T_{4'}, p_{4'})$, then determination from $\begin{cases} \text{Emec_bcle} = 0 \\ \text{Entr_bcle} = 0 \end{cases}$. When necessary, p_2 , T_2 and $T_{4'}$ then being known, the states (T_i, p_i) in the sections of the compound loop are obtained from the resolution of

$$\left\{ \begin{array}{l} \text{Emec1}_2 = 0 \\ \text{Entr1}_2 = 0 \end{array} \right. \text{ at } p_2, T_1, \text{ of } \left\{ \begin{array}{l} \text{Emec2}_3 = 0 \\ \text{Entr2}_3 = 0 \end{array} \right. \text{ at } p_3, T_3, \text{ of } \text{Entr3}_4 = 0 \text{ at } T_4, \text{ of } \text{Entr4}_4' = 0 \text{ at } p_4, \text{ and of } \left\{ \begin{array}{l} \text{Emec4}'_1 = 0 \\ \text{Entr4}'_1 = 0 \end{array} \right. \text{ at } p_1, T_1. \text{ The thermal}$$

conductances and the lengths of the pressure drops are updated at each iteration.

Solving the thermosiphon of a simple loop

It is modeled on that of the compound loop above. Main resolution is from the system (22)

$$\left\{ \begin{array}{l} \text{Emec_loop} = \sum_{e \rightarrow s} 2 \cdot g \cdot (z_s - z_e) / (v_s + v_e) - \dots \\ \dots - \sum_{e \rightarrow s} 2 \cdot w^L_{f,e \rightarrow s} / (v_s + v_e) - 2 \cdot w^r_{f_1} / (v_1 + v_2) = 0 \\ \text{Emec2}_3 = (v_2 + v_3)(p_3 - p_2) / 2 - w^L_{f,2 \rightarrow 3} = 0 \\ \text{Emec3}_4' = (v_4 + v_1)(p_4 - p_3) / 2 + g \cdot (z_4 - z_3) - w^L_{f,3 \rightarrow 4} = 0 \\ \text{Emec4}'_1 = (v_4 + v_1)(p_1 - p_4) / 2 - w^L_{f,4 \rightarrow 1} = 0 \\ \text{Entr_loop} = \sum_{e \rightarrow s} s^L_{W,e \rightarrow s} + \sum_{e \rightarrow s} s^r_{Q,e \rightarrow s} - q_{e,4 \rightarrow 1} / T_{CO} + q_{e,4 \rightarrow 1} / T_{scc} + s^r_{W} = 0 \\ \text{Entr2}_3 = -q_{e,4 \rightarrow 1} / T_{CO} + s^r_{W,2 \rightarrow 3} + s^r_{Q,2 \rightarrow 3} + (s_2 - s_3) = 0 \\ \text{Entr3}_4' = s^r_{W,3 \rightarrow 4} + s^r_{W} + (s_3 - s_4) = 0 \\ \text{Entr4}'_1 = q_{e,4 \rightarrow 1} / T_{scc} + s^r_{W,4 \rightarrow 1} + s^r_{Q,4 \rightarrow 1} + (s_4 - s_1) = 0 \\ \text{Etot4}'_1 = q_{e,4 \rightarrow 1} + (h_4 - h_1) = 0 \end{array} \right.$$

having as unknowns $M, q_{e,4 \rightarrow 1}, T_2, T_3, T_4, T_1, p_3, p_4, p_1$, and the approximate resolution from

$$\text{Eq. (21) and of the resolution of } \left\{ \begin{array}{l} \text{Emec2}_3 = 0 \\ \text{Entr2}_3 = 0 \end{array} \right. \text{ at } p_3, T_3, \text{ of } \text{Entr3}_4' = 0 \text{ at } p_4, \text{ and of } \left\{ \begin{array}{l} \text{Emec4}'_1 = 0 \\ \text{Entr4}'_1 = 0 \end{array} \right. \text{ at } p_1, T_1.$$

Calculation code and sizing

The external functioning conditions of the studied hatchery having been parameterized in the calculation code, its sizing comes down to the determination of the exchangers of the collector, of the heat discharge radiators and, for the bi-loops, of the cold loop radiator. The lengths of the elements of the wooden structure and the water reserves can be deduced from this. At the heart of these uses of the code are the troubleshooting

procedures above. A set of indices allows each of these calculations to be launched on demand.

The sizing must be performed in three successive stages, the first of which is skipped for mono-loop hatcheries: 1) determination of the thickness of the insulation of the incubator making it possible to find the cold loop radiator exchanger compensating for the positive thermals losses in scorching outdoor conditions and reduced nocturnal regeneration, 2) determination of the collector exchanger compensating for heat losses in the lowest outdoor and diurnal regeneration conditions, 3) determination of the discharge radiator exchanger maintaining the temperature at the collector outlet below the maximum operating temperature of the PVC, in the most severe diurnal regeneration condition.

The exchanger determinations are made by launching the calculation of the appropriate loop on the number of corrugations and the lengths of the exchanger chosen to approach as closely as possible the target power or temperature. Typically, a calculation by software written in Maple language occupies 10 MB and takes 3 minutes on an e-Mac.

RESULTS AND DISCUSSION

Proposed hatchery

It corresponds to a square drawer with a side of 0.456 m (six corrugations of standard corrugated iron). Its maximum capacity is 231 small chicken eggs (130 large). The maximum operating temperature of PVC is 80°C. The mono-loop and bi-loop versions are suitable for the thermal conditions found respectively under 7° latitude in Cameroon or overall, in Indonesia and between 7° and 12° latitude in Cameroon (Table 4). Their thermal design conditions, as well as their geometric and operating characteristics are brought together in Tables 5 to 7. Their material cost, estimated at 325 US dollars and 355 US dollars respectively, could bring their selling price to around 600 US dollars and 650 US dollars.

Table 4. General mean weather conditions.

Number of loops	θ'_N	θ'_J	altitudes
1	12°C ≤ ... ≤ 19°C	22°C ≤ ... ≤ 35°C	≤ 2500m
2	18°C ≤ ... ≤ 27°C	38°C ≤ ... ≤ 47°C	≤ 1500m

Table 5. External thermal conditions selected for the present sizing.

loop	$\theta'_{amb} / ^\circ\text{C}$		$\theta'_{RG} / ^\circ\text{C}$		$V_{vent} / \text{km.h}^{-1}$		$\Delta t_{RG} / \text{h}$		$\theta'_{CO} / ^\circ\text{C}$	
	mono	bi	mono	bi	mono	bi	mono	bi	mono	bi
cold	-	18	-	38	-	30	-	4	-	38.8
hot	12	18	22	38	30	30	4	4	36	36
discharge	35	47	35	47	0	0	12	12	38.8	38.8

θ_{RG} is the regeneration temperature.

Table 6. Geometric characteristics as results from the calculation point.

Number of loops	$\frac{H_{AV}}{m}$	$\frac{H_{AR}}{m}$	$\frac{L}{m}$	$\frac{l}{m}$	$\frac{L_{cap}}{m}$	$\frac{L_{inc}}{m}$	
1	1.403	1.403	1.480	0.721	0.985	0.820	
2	1.874	1.989	1.640	0.526	0.776	0.870	
Number of loops	$\frac{\tilde{L}_{CO}}{mm}$	$\frac{\tilde{l}_{CO}}{mm}$	$\frac{\tilde{h}_{CO}}{mm}$	$\frac{L_{CO}}{mm}$	$\frac{l_{CO}}{mm}$	$\frac{h_{CO}}{mm}$	$\frac{e_{isol,CO}}{mm}$
1	916	906	515				125
2	966	956	565	666	656	265	150
Number of loops	$\frac{L_N}{m}$	N_N	$\frac{L_J}{m}$	N_J	$\frac{L_D}{m}$	N_D	
1	-	-	1.50	7	1.55	18	
2	1.45	11	1.10	5	0.85	24	
Number of loops	$\frac{L_{Res,C}}{m}$	$N_{Res,C}$	$\frac{L_{Res,F}}{m}$	$N_{Res,F}$			
1	1.408	4	-	-			
2	0.976	6	0.951	2			
Number of loops	$\frac{d_{CO}}{mm}$	$\frac{D_{CO}}{mm}$	$\frac{d_{RG}}{mm}$	$\frac{D_{RG}}{mm}$	$\frac{D_{Res}}{mm}$		
1, 2	20	40	32	63	200		
Number of loops	$\frac{e_{isol,Res}}{mm}$	$\frac{e_{isol,tub}}{mm}$	$\frac{e_{bil}}{mm}$	$\frac{l_{bil}}{mm}$	$\frac{L_{bil}^{inc}}{m}$	$\frac{L_{bil}^{dech}}{m}$	
1, 2	30	0	1.4	8	1.334	4.886	

Table 7. Operating characteristics as solutions of systems (20) and (22) of the calculation point.

loop nbr	loop type	param.	state (Fig. 6)						$\frac{M}{kg}$	$\frac{\dot{Q}_e}{W}$
			1	2	3	4	4'	1'		
1	hot	$\theta/^\circ C$	51.2557	51.2556	49.2034	49.2035	49.2036	51.2558	159.9	96.6
		p/bar	1.00000	0.96106	0.96106	1.00000	1.01937	1.01934		
	disc.	$\theta/^\circ C$	-	80.7560	79.1181	-	79.1192	80.7571	1,238.	201.4
		p/bar	-	1.00000	0.99986	-	1.19303	1.19298		
2	cold	$\theta/^\circ C$	28.6881	28.6882	30.5278	30.5278	30.5277	28.6881	54.1	-29.0
		p/bar	1.00000	1.04164	1.04164	1.00000	0.98053	0.98051		
	hot	$\theta/^\circ C$	54.3410	54.3409	53.0414	53.0415	53.0416	54.3411	166.4	63.7
		p/bar	1.00000	0.95871	0.95871	1.00000	1.01933	1.01931		
disc.	$\theta/^\circ C$	-	80.1313	78.8654	-	78.8661	80.1320	848.1	106.7	
	p/bar	-	1.00000	0.99993	-	1.12651	1.12649			

Constructive provisions

The requirements of low cost, good manufacturability and availability of construction materials have led to the preference for corrugated sheet for heat exchangers and the PVC for pipes. The additional motivation for the PVC was to avoid punctures by pile effect between the metal of the pipes and that of the corrugated sheets. This led to the implementation of a heat discharge because the PVC does not withstand a

temperature higher than 60°C or 80°C depending on its type, the water easily exceeding 100°C in the event of strong insolation. The heat discharge is then done by that of the two radiators which is in the shade (Fig. 2).

A mobile and athermane separator was placed in the tanks to prevent thermal degradation by mixing the regeneration water with that from the incubator return and thus generate vigorous thermosiphons. The heat insulation of the tanks

must, moreover, be sized to make this regeneration last. The thickness adopted here (Table 6) limits the temperature drop between two successive regenerations to a few degrees.

Point 2) of the sizing (Methods Section) allows the regeneration exchangers to send the separator to the bottom of the tank under all room conditions, specially under the strongest met. The arrangement of the thermosiphon initiators, the position of the connections with the incubation sub-loop and the relative sizing of the openings and separators (Experimental Design Section) cause the thermosiphons to reverse when the separators arrive at the same end of the tank tubes, active or not sub-loop of regeneration. This results in a shuttle movement of the separators between the ends of the tank tubes which, by preventing any prolonged stagnation of the water in the tanks, also prevent ultimately the unacceptable degradation of the regeneration temperature. It should be noted that this behavior of the separator conforms to the assumptions on the calculation cycle (Methods Section).

Code validation

Figure 7 relates to the cold and hot loops of the above bi-loop hatchery. It shows how the circulation velocity and the power transferred by the thermosiphon change according to the surface area of the exchangers.

The data in Table 8 correspond to the mono-loop hatchery (Table 6) in the hot loop configuration (Table 5), except for Δt_{RG} considered equal to Δt_{cyc} and the values of θ'_j , A_j and H'_c chosen to form disparate triplets; the calculation results used for the analysis are, $\Delta\theta$, c and \dot{Q}_e .

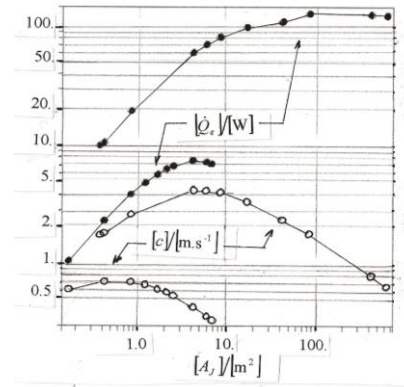


Figure 7. Changes in the flow velocity in the regeneration pipes (light circles) and the heat power transferred by the thermosiphon (dark circles) with the area of the collector (top) and the radiator (bottom).

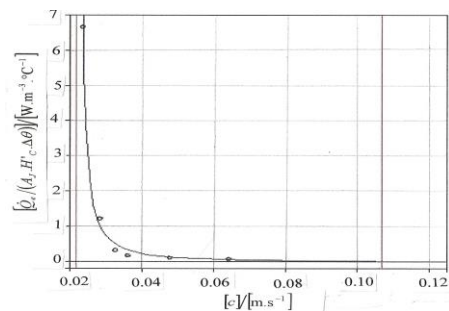


Figure 8. Specific power-water velocity correlation.

Figure 8 superimposes the points $(c, \dot{Q}_e / (A_j \cdot H'_c \cdot \Delta\theta))$ from the data in Table 8 and the curve (23)

$$\dot{Q}_e / (A_j \cdot H'_c \cdot \Delta\theta) = 0.00126 \text{ W} \cdot \text{m}^{-3} \cdot \text{s}^4 \cdot \text{C}^{-1} / (c - 0.0218 \text{ m} \cdot \text{s}^{-1})^4 - 0.0329 \text{ W} \cdot \text{m}^{-3} \cdot \text{C}^{-1}$$

which interpolates them. Its vertical asymptote in $0.0218 \text{ m} \cdot \text{s}^{-1}$ and its intersection with the abscissa axis in $0.107 \text{ m} \cdot \text{s}^{-1}$ define the functioning domain of this thermosiphon.

Table 8. Data (lines 2 to 4) and results (lines 5 to 7) of the validation study.

Point n°	$\theta'_j / ^\circ\text{C}$	A_j / m^2	H'_c / m	$\Delta\theta / ^\circ\text{C}$	\dot{Q}_e / W	$c / \text{m} \cdot \text{s}^{-1}$
1	22	1.67	1.5	128.9	104.2	0.032 4
2	50	0.59	4.25	184.0	81.03	0.035 8
3	30	3.34	2.75	146.8	156.4	0.047 5
4	40	2.51	5.00	166.7	161.8	0.064 0
5	60	0.84	0.10	205.1	115.0	0.023 4
6	35	2.09	0.35	155.9	140.2	0.028 1

Theoretical aspects

To ensure the reliability of numerical forecasts, a number of rules have been laid down. First, and contrary to the ordinary treatment of convection phenomena to which the thermosiphon is related, any approximation in the formulation of the problem, in particular the hypothesis of Boussinesq [17], was banned, which led to mobilize all the

fundamentals of classical physics: balance equation of mechanical energy (fundamental principle of dynamics), balance equations of total energy and of entropy (first and second principle of thermodynamics) without exception. Then, the ordinary model of ideal condensed body, unable of the thermosiphon by its incompressibility hypothesis, had to be replaced by the simple

thermodynamic model, and realistic between 5°C and 80°C, of liquid water developed for this study (Methods Section). Finally, to prevent foreseeable ambiguities on the results to come due to the complexity of Equations (20) and (22), the choice was made, from the outset, of a resolution by fixed point of Newton-Raphson, the solution being final since the starting point of the recurrence is in the interval of convergence of the fixed point.

A realistic modeling of the thermal aspects had to supplement these rules. The heat transfers very appreciably conditioning the temperature levels in the calorific parts of the thermosiphon and, consequently, the transferred power and the mass flow of the thermosiphon, a very particular care had to be brought in their modeling (Methods). Since radiative temperatures are not included in current meteorological data, they had to be modeled to provide correct inputs to sizing. Formula (2) derives from the observation according to which the Swinbank correlation relates to a clear sky and that of Whillier to an overcast sky [9], the first giving the values of the nocturnal radiative temperature always less than the second.

Solving the nonlinear system of 12 equations (Eq. (20)) with 12 unknowns M , $q_{e,4' \rightarrow T}$, T_1 , T_2 , T_3 , T_4 , $T_{4'}$, T_r , p_2 , p_3 , p_4 , p_r by a fixed point method nevertheless presents a real difficulty. The entanglement of the multiple phenomena in play (expansion, gravity, heat transfer, dissipation, thermal irreversibility) causes the narrowing of the interval of convergence, to the point that the starting values of the unknowns must be given in an interval often lower than a tenth of their value. Adding to this the fact that they are highly dependent on the problem under study, it was unthinkable to seek to fix them once and for all for any type of problem. The major challenge of this study has been the shaping of a starting point sufficiently close to the fixed point.

It was noted by calculating the starting values by an approximate resolution (Methods Section) based on the idea that water would be assumed to be an ideal condensed body as long as this would not call into question the thermosiphon, and that the fundamentals of the phenomenon: loop balances of mechanical energy, total energy and entropy had to be respected. Multiple subsequent numerical implementations have shown that this method generally leads to the values close enough to the fixed point to solve, with 20 significant digits, Eq. (20) to better than 10^{-14} in SI units, so that when the calculation of fixed point results in unacceptable negative or complex values, one can conclude that the problem does not admit a physical solution.

Numerical validation results

With Reynolds numbers still below 2 000 in pipe, numerical simulations confirmed the laminar flow hypothesis (Methods).

The difficulty in solving the thermosiphon appeared in the 20 significant digits necessary for the calculations and the time ratio of the approach and fixed-point calculations (11 in a compound loop).

The domains in which the exchange surfaces have been sought (Methods) are visible in Fig. 7 (log-log coordinates to make the changes in hot and cold loops comparable). They correspond to the points without calculation anomaly: at low values of the exchange surface, the calculation fails, in fact, as a result of violations of the second principle and at high values, it alternates between the normal and an unbridled regime. The evolutions are, moreover, in accordance with the intuition of the thermosiphon phenomenon, the transferred power being generally increasing with the surface and the velocities of flow, with an extremum. Given the difference in the configurations studied, the orders of magnitude are compatible with those reported in the literature on thermosiphon solar collectors [18, 19, 20, 21].

To push these investigations further, we fixed the disparate data from Table 8, the representation of which appears in the form of a plane point cloud in any combination other than $(c, \dot{Q}_e / (A_J \cdot H'_c \cdot \Delta\theta))$. The strong improbability of connecting these five variables in a single correlation, their grouping in the end in the vicinity close to an elementary curve (Fig. 8) and the regular functioning of the thermosiphon in a limited domain seem to indicate that the physics of the phenomenon have been captured. We can therefore expect to have fairly accurate forecasts, in excellent trends. Obviously, the verdict regarding their accuracy will only be given by comparison with *in-situ* measurements.

CONCLUSION

The tropical and equatorial countries are particularly favored to constitute, by solar collection and nocturnal radiative emission, in all seasons, water reserves at temperature levels suitable for heating or cooling an incubator. The solutions described above are certainly the most suitable for making sustainable and fair-trade use of these free and inexhaustible heat resources.

The proximity of Indonesia's territories to the ocean attenuates the amplitude of thermal variations and maintains their level below 36°C. As a result, Indonesian fair-trade hatcheries would not have a cold loop and their water reserve would be

less massive. This is the only specificity of Indonesian hatcheries compared to the Cameroonian ones.

The circulation of water by thermosiphon and regulation by bimetallic strip will relieve operators from the constraint of using a generator or investing in photovoltaics [1] to compensate for the shortcomings of the electrical network, incubation by commercial hatcheries, solar or not, tolerating neither the absence nor the prolonged interruption of electric current.

The horizontal position of the collector is that which maximizes solar collection in all seasons at low latitudes. Likewise, the horizontal position of the radiator in bi-loop hatcheries maximizes radiative emission, especially in clear nocturnal sky of tropical regions.

The incubator's egg drawer is the centerpiece of the hatchery. The three functions assigned to it: maintaining the eggs at a uniform temperature within the non-suffering interval of the embryos, immersion in a humid atmosphere and easy turning, are correctly carried out here. The envelope has been internally insulated to achieve the rigorous thermal insulation required by the low heat powers transferred by the thermosiphons.

Fair-trade sustainable hatcheries of larger capacity than the one proposed have been sized, but their size makes them difficult to handle the drawer of eggs and uncertain their solidity. As for the smaller one, with a material cost close to 300 US dollars, it was deemed commercially unattractive. Regarding the proposed hatchery, its material cost has been minimized on the thickness of the incubator insulation.

The investments, reduced to the approved egg, of the fair-trade sustainable hatchery (600 US dollars, 231 eggs) and of a commercial one (3 000 US dollars, 1 000 eggs, 650 W) are equivalent: 2.6 and 3.0 US dollars/egg, respectively. However, the operation of the latter cannot be done without electrical back-up. We find that, at the rate of 17 broods per year and over an amortization period of 5 years, the cost price of the day-old chick is here 0.04 US dollars against 0.26 US dollars (kWh at 0.50 US dollars). It should be noted that, based on an annual income of around 9, 000 US dollars (day-old chick sold at 0.77 US dollars), the operation of three fair-trade sustainable hatcheries already corresponds to a small hatching company.

Finally, it cannot be imagined that hatcheries based on the present principle, well suitable to extreme given conditions without, however, being oversized, could have been developed by a purely empirical route in reasonable time and at reasonable cost. The computer code and through it, the elaborate physical model of the complex

thermosiphon, were the masterpiece of their design.

REFERENCES

- [1]. M. Djamin, A. S. Dasuki, A. Y. Lubis and F. Alyuswar. 2001. Application of photovoltaic systems for increasing villager's income. *Renewable Energy*, 22 1-3: 263-267.
- [2]. J. Retamozo, F. J. Rojas. 2022. Design and economic analysis of a solar poultry incubator for rural sectors located in Pucallpa-Peru. *Renewable Energy and Power Quality Journal*, 20: 318-323.
- [3]. S. C. Ikpeseni, K. Owebor, H. I. Owamah, S. O. Sado, D. E. C. Odeh. 2022. Design and Fabrication of a Local Solar Powered Poultry Egg Incubator for a Low-Income Country. *Journal of the Institution of Engineers (India). Series B*, 103 3: 779-790.
- [4]. A. Carillo Andrés, J. M. Cejudo Lopez. 2002. TRNSYS model of a thermosiphon solar domestic water heater with a horizontal store and mantle heat exchanger. *Solar Energy*, 72 2: 89-98.
- [5]. M. J. Alshukri, A. K. Hussein, A. A. Eidam, A. I. Alsabery. 2022. A review on applications and techniques of improving the performance of heat pipe-solar collector systems. *Solar Energy*, 236: 417-433.
- [6]. D. Brough, J. Ramos, B. Delpech, H. Jouhara. 2021. Development and validation of a TRNSYS type to simulate heat pipe heat exchangers in transient application of waste heat recovery. *International Journal of Thermofluids*, 100056.
- [7]. A. Lourens, H. van den Brand, R. Meijerhof and B. Kemp. 2005. Effect of Eggshell Temperature During Incubation on Embryo Development, Hatchability, and Posthatch Development. *Poultry Sciences*, 84, 914-920.
- [8]. A. A. Sfeir, G. Guarracino. 1981. Ingénierie des systèmes solaires. Technique & Documentation Lavoisier. Paris.
- [9]. M. Feidt. 2016. Conversion thermosolaire. p. 429. *In: Thermodynamique et optimisation énergétique des systèmes et procédés*. Tec & doc Lavoisier. Paris.
- [10]. J. Jouanneau. 1985. Pyromètres à bilames. p. 9 *In: Techniques de l'Ingénieur*. R 2540.
- [11]. A.-M. Bianchi, Y. Fautrelle, J. Etay. 2004. Transferts thermiques. Presses Polytechniques et Universitaires Romandes. Lausanne.
- [12]. J. A. Dean. 2005. Physical properties. P5. 155. *In: Mc Graw-Hill Handbooks. Lange's Handbook of Chemistry*, 16th Ed. Mc Graw Hill. New York.

- [13]. L. Borel, D. Favrat. 2005. Généralités et principes fondamentaux. p. 23. *In: Thermodynamique énergétique tome 1*, Presses Polytechniques et Universitaires Romandes. Lausanne.
- [14]. L. Borel, D. Favrat. 2005. Généralités et principes fondamentaux. p. 48. *In: Thermodynamique énergétique tome 1*, Presses Polytechniques et Universitaires Romandes. Lausanne.
- [15]. I. E. Idel'cik. 1986. Mémento des pertes de charge. Collection de la Direction des Études et Recherches d'Électricité de France. 3^{ème} édition. Eyrolles Éditeur. Paris.
- [16]. A. F. Izmailov, M. V. Solodov. 2014. Newton-type methods for optimization and variational problems, Springer series in Operations Research and Financial Engineering. Springer.
- [17]. A.-M. Bianchi, Y. Fautrelle, J. Etay. 2004. Convection naturelle. p.192. *In: Transferts thermiques*. Presses Polytechniques et Universitaires Romandes. Lausanne.
- [18]. J. A. Khalid, F. Basim, A. M. Hamed. 2021. Numerical and experimental investigation of a thermosiphon solar water heater system thermal performance used in domestic application. *Heat Transfert*, 50 (5) 4575-4594.
- [19]. K. Chuawittayawuth and S. Kumar. 2002. Experimental investigation of temperature and flow distribution in a thermosiphon solar water heating system. *Renewable Energy*, 26 (3) 486-488.
- [20]. M. Azzolin, A. Mariani, L. Moro, A. Tolotto, P. Toninelli and D. Del Col. 2018. Mathematical model of a thermosiphon integrated storage solar collector. *Renewable Energy*, 128 (A) 400-415.
- [21]. A. Zerrouki, A. Boumédién and K. BouhadeF. 2002. The natural circulation solar water heater model with linear temperature distribution. *Renewable Energy*, 26 (4) 549-559.